Research in Pharmaceutical Sciences, June 2025; 20(3): 373-391
Received: 27-12-2024
Peer Reviewed: 22-01-2025
Revised: 25-03-2025
Accepted: 13-04-2025
Published: 17-06-2025

School of Pharmacy & Pharmaceutical Sciences
Isfahan University of Medical Sciences

Original Article

Expression and functional characterization of an anti-CD22 scFv targeting B-cell malignancies

Monireh Gholizadeh[1,2], Shahriyar Abdoli[3], Shafieeh Mansoori[2], Arash Arashkia[4], Farhad Riazi-Rad[2], Amir Ali Hamidieh[5], Mohammad Nouri[1,*], and Zahra Sharifzadeh[2,*]

[1]*Department of Medical Biotechnology, Faculty of Advanced Medical Sciences, Tabriz University of Medical Sciences, Tabriz, Iran.*
[2]*Department of Immunology, Pasteur Institute of Iran, Tehran, Iran.*
[3]*School of Advanced Medical Technologies, Golestan University of Medical Sciences, Gorgan, Iran.*
[4]*Department of Molecular Virology, Pasteur Institute of Iran, Tehran, Iran.*
[5]*Pediatric Cell and Gene Therapy Research Center, Gene, Cell & Tissue Research Institute, Tehran University of Medical Sciences, Tehran, Iran.*

Abstract

Background and purpose: Single-chain variable fragments (scFvs) offer advantages over full-length monoclonal antibodies in cancer therapy, including reduced size, lower production costs, and easier handling. However, *Escherichia coli* (*E. coli*) often leads to the formation and aggregation of inclusion bodies (IBs). This study aimed to optimize the expression and purification of an anti-CD22 scFv (CD22-scFv) in *E. coli* and evaluate its functional properties.

Experimental approach: The CD22-scFv construct was subcloned into pET-28a(+) and expressed in *E. coli* strains Rosetta (DE3) and Rosetta-gami 2. To overcome IBs formation, two purification methods were employed to enhance soluble protein production: hybrid conditions, a novel one-step immobilized metal affinity chromatography (IMAC)-based on-column refolding method was employed, using gradually decreasing urea and increasing imidazole concentrations; native conditions, expression parameters (IPTG concentration, post-induction temperature, and time) were optimized, followed by IMAC. The CD22-scFv binding to CD22 antigen and its anti-proliferative effects on target cells were assessed *via* flow cytometry and MTT assay.

Findings/Results: CD22-scFv was successfully expressed in Rosetta (DE3) but not Rosetta-gami 2. Hybrid purification yielded 15.86 mg/L protein, outperforming native purification (3.65 mg/L). Flow cytometry confirmed the binding of native- and hybrid-purified CD22-scFv to CD22 Raji cells with 75.5% and 55.8% efficiency, respectively. Native-purified CD22-scFv significantly inhibited Raji cell proliferation while sparing $CD22^{-}$ cells.

Conclusion and implications: This study established a scalable and cost-effective strategy for producing functional CD22-scFv with high specificity and anti-proliferative effects. The findings highlight its potential for targeted therapies and diagnostics, warranting further *in vivo* and clinical studies.

Keywords: CD22-scFv; *E. coli* expression system; IMAC purification; Immunotherapy; On-column refolding; Protein solubility.

INTRODUCTION

Hematological malignancies (HMs) encompass a diverse group of cancers classified into four major categories: leukemia, non-Hodgkin lymphoma, Hodgkin lymphoma, and multiple myeloma (1). Since 1990, the global incidence of HMs has steadily increased, reaching approximately 1.34 million cases in 2019.

*Corresponding authors:
Z. Sharifzadeh, Tel: +98-9128200112, Fax: +98-216649259
Email: zsharifzadeh@gmail.com
M. Nouri, Tel: +98-9144054268, Fax: +98-4133368890
Email: Nourimd@yahoo.com

Access this article online

Website: http://rps.mui.ac.ir

DOI: 10.4103/RPS.RPS_248_24

Sustained advancements in preventative measures, early diagnostic techniques, and therapeutic interventions have obviously contributed to a reduction in mortality rates associated with a spectrum of HMs (2). Although chemotherapy and radiotherapy remain cornerstones of cancer treatment, their therapeutic efficacy is often constrained and frequently accompanied by substantial adverse effects (3). Developed in the 1980s, biopharmaceuticals represent a major advancement in modern science (4), offering highly effective treatment options across various medical fields, including cancer (5). Biopharmaceutical products encompass a range of therapeutic agents, such as monoclonal antibodies (mAbs), recombinant proteins, or vaccines, which are developed using biotechnological methods, including recombinant DNA technology (6). Among the most biopharmaceutical products, mAbs and their derivatives are recognized for their high therapeutic potential and have been widely utilized in the treatment of various conditions, including cancer (5). Despite offering high therapeutic efficiency, sensitivity, and specificity, the widespread clinical application of mAbs is often hindered by challenges such as limited stability (7), aggregation (8), and post-translational modifications (PTMs), including glycosylation and oxidation (9). Due to their large size, the poor tissue penetration of mAbs represents a significant limitation, particularly in solid tumors. To address this issue, researchers have developed single-chain variable fragments (scFvs), composed of the variable regions of antibody light (VL) and heavy (VH) chains connected by a flexible polypeptide linker. ScFvs retain the antigen-binding specificity of full-length mAbs (10,11) and offer several advantages, including smaller size, enhanced tissue penetration, rapid clearance, and reduced immunogenicity due to the absence of the Fc region (12).

The production of scFvs employs various expression systems, including prokaryotic and eukaryotic (mammalian, fungal, or insect cell lines) platforms (4). Among these, *Escherichia coli (E. coli)* remains the preferred prokaryotic system due to its cost-effectiveness, rapid growth, high productivity, and well-characterized biochemistry and genetics (13). *E. coli* has been successfully utilized for the production of various recombinant proteins, including scFvs, HBsAg-polyepitope constructs, and granulocyte-macrophage colony-stimulating factor (GM-CSF) cytokine (14,15). However, the *E. coli* expression system presents several challenges, including coding bias, lack of PTMS, and endotoxin problems (13). Additionally, a significant limitation is the frequent formation of inclusion bodies (IBs), insoluble protein aggregates within the bacterial cytoplasm, particularly when overexpressing heterologous proteins (12,16-20). The formation of IBs is a frequently encountered challenge for producing soluble and functional recombinant proteins. Researchers have developed various approaches to overcome this hurdle, including optimizing expression conditions, co-expression with molecular chaperones, using fusion tags to enhance solubility, and engineering *E. coli* strains for improved protein folding and reduced IB formation. Specifically, optimizing expression conditions involves adjusting diverse parameters such as the choice of expression strain, inducer concentration, post-induction time, and post-induction temperature, all of which play key roles in influencing the yield and solubility of expressed proteins (21,22).

The immobilized-metal affinity chromatography (IMAC) is a widely recognized and effective technique for purifying proteins from recombinant microorganisms (23). Its low cost, simplicity, and ability to operate under native and denaturing conditions position IMAC as a highly versatile chromatographic method. This unique capability allows for the renaturation of proteins directly on the column, ensuring proper folding while minimizing aggregation (24). Thus, the technique has recently emerged as a promising strategy for improving recombinant protein production. This technique isolates His-tagged proteins using metal ion-chelated resins while facilitating proper protein folding by gradually removing denaturing agents such as urea. Specifically, the method combines a stepwise reduction in urea concentration with a concurrent increase in imidazole concentration, enabling the

simultaneous purification and refolding of proteins from IBs. By maintaining the protein in a controlled environment during the renaturation process, this approach minimizes aggregation and enhances the yield of correctly folded proteins. Compared to conventional renaturation methods such as dilution and dialysis, this technique offers superior efficiency and economic advantages by integrating the purification and refolding processes into a single step. The IMAC-based on-column refolding and purification method presents a cost-effective and efficient solution for recombinant protein production. This streamlined approach significantly reduces processing time and resource utilization while enhancing scalability, making it suitable for industrial-scale protein production (25,26).

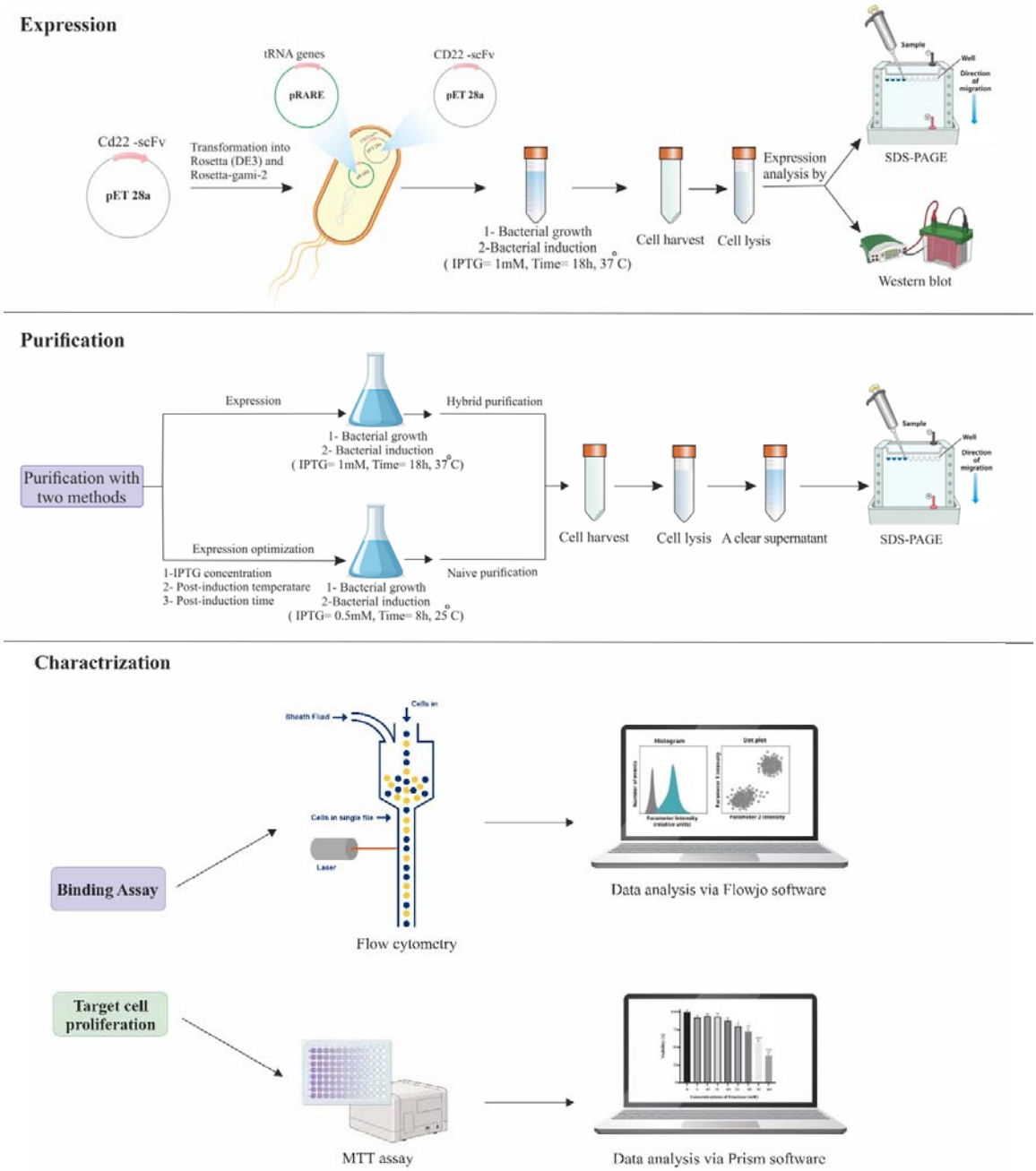

Fig. 1. Schematic representation of the workflow used for the expression, purification, and characterization of the CD22-scFv protein.

We focused on developing and optimizing a scFv targeting CD22 (CD22-scFv), a cell surface marker predominantly expressed on B cells. CD22 is a key regulator of B-cell function and homeostasis, making it an ideal target for precision therapies aimed at treating B-cells in hematological malignancies such as non-Hodgkin lymphoma and acute lymphoblastic leukemia. Given its critical involvement in B-cell malignancies, CD22-specific therapeutics hold considerable promise for improving treatment outcomes in these cancers.

Our primary objective was to optimize the production and purification of soluble CD22-scFv in *E. coli* using two distinct approaches. To achieve this, a CD22-scFv construct was designed and synthesized in the pUC18 vector by Biomatik. The CD22-scFv was subsequently subcloned into the pET28a vector and expressed in two strains of *E. coli Rosetta*. The formation of IBs was confirmed. Consequently, two independent methods were employed for protein purification. The first approach involved purification under hybrid conditions using an IMAC-based on-column refolding method. The second approach focused on purification under native conditions by optimizing expression parameters, including isopropyl β-D-1-thiogalactopyranoside (IPTG) concentration, post-induction temperature, and post-induction time, to maximize soluble protein production. Proteins expressed under native conditions were subsequently purified using IMAC with imidazole-based buffers. We then evaluated the functional properties of the hybrid-purified and native-purified CD22-scFvs, including their antigen-binding efficiency and anti-proliferative effects on $CD22^+$ tumor cells. The binding ability of the purified recombinant proteins to target cells was evaluated using flow cytometry. Additionally, the impact of CD22-scFv on the proliferation of the $CD22^+$ Raji cell line was assessed using the 3-(4,5-dimethylthiazol-2-yl)-2,5-diphenyltetrazolium bromide (MTT) assay. Figure 1 illustrates the stepwise approach employed in this study to express, purify, and characterize the CD22-scFv protein.

MATERIALS AND METHODS

Design and synthesis of the CD22-scFv construct

The CD22-scFv construct, consisting of VH-linker-VL CD22-scFv, a Flag-tag, and a His-tag, was designed using CLC Genomics Workbench 20 software and synthesized by Biomatik in the pUC18 vector. The sequence of the CD22-scFv (m971) was derived from U.S. Patent No. US10,072,078 B2 (September 11, 2018), attributed to inventors Dr. Rimas J. Orentas *et al*.

Subcloning of CD22-scFv gene into pET-28a (+) vector and screening of recombinants

The CD22-scFv-pUC18 plasmid was extracted and digested with *Xho*I and *Bam*HI restriction enzymes. The desired fragment was then gel-extracted using a Gel Extraction Kit (Bio Basic Inc., Canada). Similarly, the pET-28a (+) expression vector was extracted and digested with *Xho*I and *Bam*HI. The linearized vector was gel-extracted. Ligation of the linearized pET-28a (+) expression vector and the CD22-scFv fragment was performed using T4 DNA Ligase. The resulting CD22-scFv-pET-28a (+) expression vector was transformed into chemically competent TOP10F' *E. coli* cells *via* heat shock. Subcloning was confirmed by extracting the plasmid (Qiagen, Netherlands) from selected clones and performing enzymatic digestion with the *Pvu*II restriction enzyme.

Expression and identification of CD22-scFv protein

The confirmed plasmid was transformed into two *E. coli* strains, Rosetta (DE3) (Invitrogen, USA) and Rosetta-gami-2 (Invitrogen, USA), *via* heat shock. For each strain, two clones were selected for protein expression assays. Expression of CD22-scFv was conducted at 37 °C for 18 h in 10 mL of super optimal broth with catabolite repression (SOC) media containing 30 µg/mL kanamycin with shaking (200 rpm). Cultures were induced with 1 mM IPTG when an optical density (OD) of 0.6 at 600 nm was reached. Cells were harvested by centrifugation (20 min, 4 °C, 4000 *g*), and lysed using lysis buffer (300 mM NaCl, 10 mM imidazole (Merck, Germany), and 1x phosphate-buffered saline (PBS), adjusted to pH 8.0 using NaOH 1M) supplemented with 1% (v/v) phenylmethylsulfonyl fluoride (PMSF; Merck KGaA, Darmstadt, Germany) and 0.1% lysozyme (Sigma-Aldrich Chemie GmbH, Germany). Expression samples were analyzed *via* 12% sodium dodecyl-sulfate

polyacrylamide gel electrophoresis (SDS-PAGE) followed by Coomassie brilliant blue staining. To confirm CD22-scFv protein expression, western blot analysis was performed. Protein samples were separated on an acrylamide gel and transferred to a polyvinylidene difluoride (PVDF) membrane (Sigma Aldrich, Germany). The PVDF membrane was incubated with a 1:500 dilution of anti-His-tag antibody conjugated with horseradish peroxidase (HRP) enzyme (Sina Biotech, Iran), washed twice with PBS buffer, and washed twice with PBS-tween buffer. Finally, a 3,3'-diaminobenzidine (DAB) solution was added to the PVDF membrane to visualize protein bands.

Solubility determination of CD22-scFv protein

Following the Qiagen purification protocol, 50 mL of pre-warmed SOC media containing kanamycin was inoculated with 2.5 mL of overnight cultures and incubated at 37 °C/200 rpm until the OD_{600} reached approximately 0.6. A 1 mL sample was taken before induction as a non-induced control and the cells were pelleted and resuspended in 100 µL 1x SDS-PAGE sample buffer. Expression was induced by adding IPTG to a final concentration of 1 mM. After 4 h of growth at 37 °C/200 rpm, a second 1 mL sample was collected as an induced control. The cell pellets were centrifuged and resuspended in 100 µL 1x SDS-PAGE sample buffer. The remaining culture was centrifuged (20 min, 4 °C, 4000 *g*). The cell pellet was then resuspended in 5 mL of lysis buffer for purification under native conditions (Table S1), supplemented with 1% PMSF and 0.1% lysozyme, and incubated on ice for 30 min. The lysates were sonicated and clarified by centrifugation (30 min, 4 °C, 10000 *g*). The supernatant was collected as the crude extract A (soluble protein sample). The remaining cell pellet was resuspended in 5 mL lysis buffer and used as the crude extract B (insoluble protein sample). Finally, the fractions were analyzed by 12% SDS-PAGE.

scFv-CD22 protein purification under hybrid conditions

For purification under hybrid conditions, 200 mL of pre-warmed SOC medium was inoculated with 10 mL of overnight bacterial culture and incubated at 37 °C/200 rpm until the OD reached approximately 0.6 to 0.7. IPTG was added to a final concentration of 1 mM and the culture was incubated at 37 °C /200 rpm for 18 h. Following centrifugation at 4000 *g* for 20 min/4 °C, cell pellets were lysed using lysis buffer (Table S2) supplemented with 1% PMSF and 0.1% lysozyme, sonicated (20 cycles of 10s with 15 s pauses at 250 W), and clarified by centrifugation (30 min, 4 °C, 10000 *g*). The clarified supernatant was applied to a Ni-NTA affinity chromatography column containing 2 mL of agarose bead technology (ABT) resin (Madrid, Spain) that had been equilibrated with lysis buffer (Table S2). The supernatant and Ni-NTA resin were gently mixed by shaking for 90 min. The column was washed twice with 15 mL of washing buffers 1 through 5, respectively (Table S2), generating wash samples 1-10. Bound protein was eluted twice with 2 mL of elution buffer 1 (Table S2) to produce elution samples 1 and 2, and three times with 2 mL of elution buffer 2 (Table S2) to generate elution samples 3, 4, and 5. Collected fractions were analyzed using 12% SDS-PAGE.

Effects of inducer concentration on soluble expression of CD22-scFv protein

Following the Qiagen purification protocol, 50 mL of pre-warmed SOC media containing kanamycin was inoculated with 2.5 mL of overnight cultures and incubated at 37 °C/200 rpm until the OD_{600} reached approximately 0.6. A 1 mL sample was immediately taken before induction as a non-induced control. Various IPTG concentrations (0.05, 0.1, 0.2, 0.5, 0.75, and 1 mM) were added, and a second 1 mL sample was taken as an induced control after the cultures were grown for an additional 4 h. The cell pellets were centrifuged and resuspended in 100 µL of 1x SDS-PAGE sample buffer. The remaining culture medium was centrifuged (20 min, 4 °C, 4000 *g*). For purification under native conditions, the cell pellet was resuspended in 5 mL of lysis buffer (Table S1), supplemented with 1% PMSF and 0.1% lysozyme, and incubated on ice for 30 min. The lysates were sonicated and clarified by centrifugation (30 min, 4 °C, 10000 *g*). The clarified supernatant was collected as the crude

extract A (soluble protein sample). The remaining pellet was resuspended in 5 mL lysis buffer and used as the crude extract B (insoluble protein sample). Finally, the collected fractions were analyzed by 12% SDS-PAGE.

Effects of post-induction temperature and time on soluble expression of CD22-scFv protein

Fifty mL of prewarmed SOC media containing kanamycin was inoculated with 2.5 mL of the overnight culture and incubated at 37 °C/200 rpm until the OD_{600} reached approximately 0.6. The culture was then divided into six 6-mL aliquots, each induced with 0.5 mM IPTG and incubated at 37 °C/200 rpm for 2, 4, 6, 8, and 18 h. After incubation, cells were harvested by centrifugation and subsequent steps were performed as described. The protein concentration of the fractions was determined according to the absorbance of samples at 280 nm measured with a NanoDrop spectrophotometer. Cell pellets and supernatant samples from each experiment were then analyzed using 12% SDS-PAGE.

The aforesaid steps were repeated for simultaneous optimization of induction temperatures (20, 25, and 30 °C). After OD reached 0.6, the cultures were placed on ice for 20-30 min to lower the temperature of the medium before induction with 0.5 mM IPTG.

CD22-scFv protein purification under native conditions

One hundred mL of pre-warmed SOC medium was inoculated with 5 mL of overnight bacterial culture of the recombinant clone and incubated at 37 °C/200 rpm. After OD reached 0.6, the culture was placed on ice for 20-30 min to reduce the temperature, induced with 0.5 mM IPTG, and incubated for 8 h at 25 °C/200 rpm. Cells were harvested by centrifugation (30 min, 4 °C, 4000 *g*), and the cell pellets were lysed by lysis buffer (Table S1) supplemented with 1% PMSF and 0.1% lysozyme, sonicated (10 cycles of 7 s with 10 s pauses at 250 W), and clarified by centrifugation (30 min, 4 °C, 10000 *g*). The supernatant was used for Ni-NTA affinity chromatography using 1 mL of ABT resin (Qiagen, Netherlands) that had been equilibrated twice with 10 mL of equilibration buffer (Table S1). The supernatant and Ni-NTA resin were gently mixed by shaking at 4 °C for 70 min. The column was washed twice with 7 mL of washing buffers 1 and 2, respectively (Table S1), generating wash samples 1-4. Bound protein was eluted twice with 750 µL of elution buffer 1 (Table S1) to produce elution samples 1 and 2, and twice with 750 µL of elution buffer 2 (Table S1) to generate elution samples 3 and 4. Collected fractions were analyzed using 12% SDS-PAGE.

Flow cytometry binding analysis

The initial assessment of CD22 surface expression on $CD22^+$ Raji and $CD22^-$ K562 cells was conducted utilizing PE anti-CD22 antibody (BD Biosciences, USA), purchased from the National Cell Bank of Iran (NCBI, Pasteur Institute of Iran, Tehran, Iran). Subsequently, these cells were used to study the specific binding of the purified CD22-scFv proteins. CD22 expression on Raji and K562 cells was confirmed using a commercial anti-CD22 antibody *via* flow cytometry. To prevent $CD22^-$scFv internalization, 1×10^6 Raji and K562 cells were fixed with 4% formaldehyde at room temperature for 15 min and washed once with 1000 µL of fluorescence-activated cell sorting (FACS) buffer (PBS, 2% FBS, and 0.1% NaN3). Cells were then incubated on ice for 60 min in 0.5 mL of 10% human serum to block Fc receptors, washed once with 1000 µL of FACS buffer, and resuspended in 100 µL FACS buffer containing 2 µg of CD22-scFv proteins purified under native and hybrid conditions for 60 min at 4 °C. Cells were pelleted, washed once with 1000 µL of FACS buffer, and incubated in 100 µL FACS buffer containing 1 µg mouse anti-FLAG-tag (Sigma-Aldrich Chemie GmbH, Germany) as the primary antibody for 30 min in the dark at 4 °C. Following a wash with 1000 µL of FACS buffer, cells were incubated in 100 µL of FACS buffer containing 1 µg of FITC anti-mouse IgG antibody (BioLegend, USA) as the secondary antibody for 30 min in the dark at 4 °C. Finally, cells were washed twice using 1000 µL of FACS buffer to eliminate unbound antibodies. Samples were analyzed by flow cytometry using a Partec PAS III flow cytometer (Partec GmbH, Görlitz, Germany), and data were processed with FlowJo software (Tree Star, Inc., Ashland, OR, USA).

Evaluation of CD22$^+$ Raji cell proliferation following binding of CD22-scFv

The MTT assay was used to evaluate the impact of CD22-scFv binding on the proliferation of CD22$^+$ Raji cells. Briefly, 1 × 10^5 cells/well Raji or K562 cells were incubated in a 96-well plate with various concentrations of CD22-scFv (1, 4, and 8 µg/mL) purified under native conditions at 37 °C, 5% CO_2 for 48 h. Untreated cells were used as the control (100 % viable cells). The 96-well plate was centrifuged (650 g/8 min/30 °C) and the media was discarded. Subsequently, 20 µL stock solution of MTT reagent (5 mg/mL in PBS) was added to 100 µL phenol red-free Roswell Park Memorial Institute medium (RPMI)-1640 to achieve a final concentration of 0.83 mg/mL in each well. Plates were then incubated at 37 ℃ for 3 h. After removing the supernatant by centrifugation (650 g/8 min/30 °C), DMSO (100 µL/well) was added and shaken for 10 min to dissolve formazan. Each sample, with three replicates, was analyzed on a microplate reader at 570 nm with a reference wavelength of 690 nm using the BioTek ELx808 Absorbance Microplate Reader (BioTek Instruments, USA).

Statistical analysis

All quantitative data are presented as mean ± SD. Statistical comparisons among groups were carried out using one-way analysis of variance (ANOVA). *P*-values < 0.05 were considered statistically significant. All statistical analyses and graphical visualizations were performed using GraphPad Prism version 10.4.1 (GraphPad Software, San Diego, CA, USA).

Supplementary materials

Table S1 and Table S2 are available *via* the link below:

Tables S1 & S2-Expression and functional characterization of an anti-CD22 scFv targeting B-cell malignancies.docx

RESULTS

Subcloning of the CD22-scFv gene and screening of recombinant colonies

Digestion of the CD22-scFv-pUC18 vector yielded two fragments of approximately 2600 bp and 800 bp (Fig. 2A). Similarly, digestion of the pET-28a (+) expression plasmid resulted in a 5333-bp linearized vector, which was also gel-extracted (Fig. 2B). Successful subcloning into the pET-28a (+) expression plasmid was confirmed by digestion, resulting in fragments of 3311 bp, 1781 bp, and 999 bp (Fig. 2C). Schematic diagram of the CD22-scFv-pET28a+ plasmid for *E. coli* expression and the restriction enzyme sites of *Xho*I, *Bam*HI, and *Pvu*II were shown in Fig. 2D.

CD22-scFv expression

SDS-PAGE analysis revealed that Rosetta (DE3) clones consistently achieved the highest expression levels, as indicated by a distinct band at approximately 38 kDa (Fig. 3A). This band corresponds to the expected molecular weight of CD22-scFv. Rosetta-gami-2 clones exhibited significantly lower expression levels under the same conditions (Fig. 3B). Western blot analysis using an anti-His-tag-HRP antibody corroborated these findings, confirming robust CD22-scFv expression in Rosetta (DE3) clones, with minimal to no expression detected in Rosetta-gami-2 clones (Fig. 4A and B).

Solubility analysis of CD22-scFv protein

The solubility of CD22-scFv was evaluated according to the Qiagen purification protocol, and samples were analyzed by SDS-PAGE (Fig. 5). The Rosetta (DE3) cells without the expression plasmid (negative control) exhibited no bands corresponding to CD22-scFv (Fig. 5, Lane 2), confirming the absence of background expression. Similarly, the non-induced control showed no recombinant protein (Fig. 5, Lane 6), indicating that protein expression was strictly IPTG-dependent. Following IPTG induction, a distinct band corresponding to CD22-scFv was observed (Fig. 5, Lane 3). The soluble fraction (crude extract A) analysis revealed no detectable CD22-scFv (Fig. 5, Lane 4), indicating minimal solubility under native conditions. Conversely, a strong band at ~38 kDa (Fig. 5, Lane 5) was observed in the insoluble fraction (crude extract B), demonstrating that most expressed protein was present in IBs.

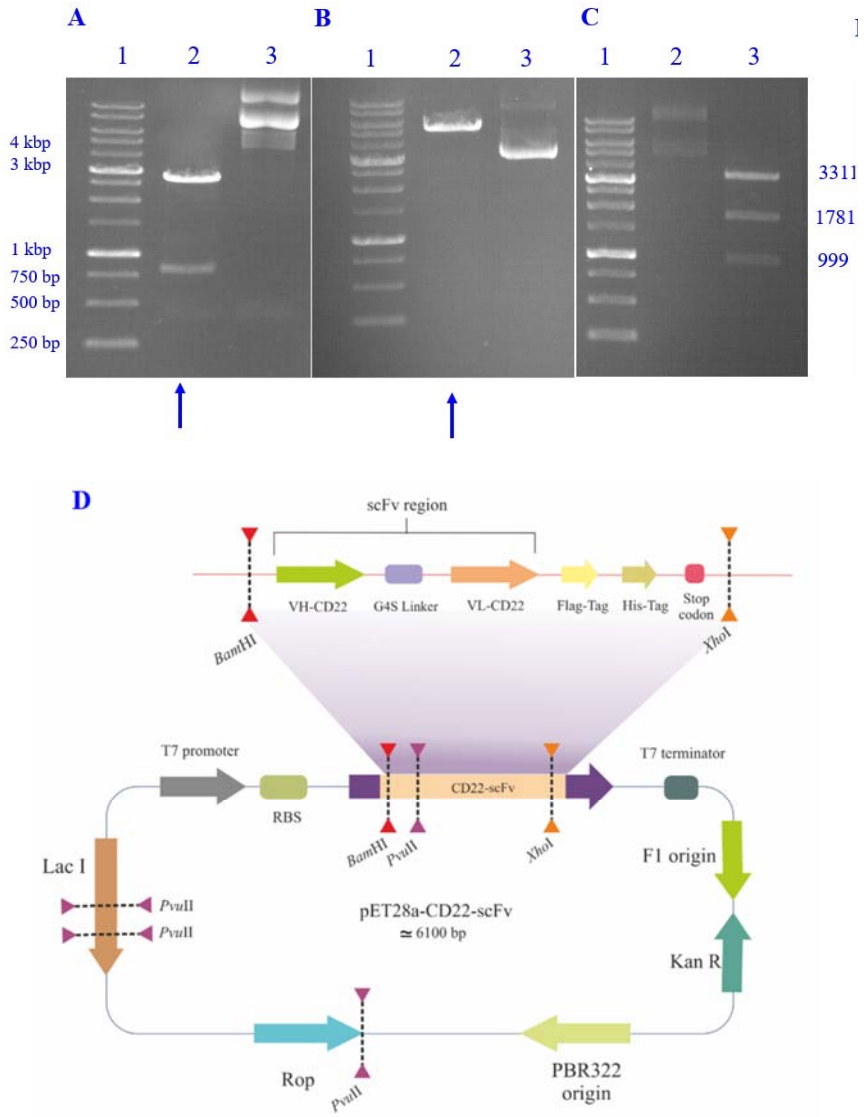

Fig. 2. Validation of CD22-scFv subcloning into the pET-28a(+) expression vector. (A) Restriction digestion analysis of the CD22-scFv-pUC18 vector using *Xho*I and *Bam*HI, resulting in two fragments of approximately 2600 bp and 800 bp, confirming the successful insertion of the CD22-scFv gene into the pUC18 vector. Lane assignments: 1-kbp marker (Lane 1), digested pUC18 vector (Lane 2), and undigested plasmid control (Lane 3). (B) Restriction digestion analysis of the pET-28a(+) vector using *XhoI* and *BamHI*, yielding a linearized fragment of 5333 bp, which was subsequently ligated with the CD22-scFv insert. Lane assignments: 1-kbp DNA ladder (Lane 1), digested pET-28a(+) vector (Lane 2), and undigested plasmid control (Lane 3). (C) Restriction digestion analysis of the recombinant pET-28a(+)-CD22-scFv construct with *PvuII*, resulting in three fragments of 999 bp, 1781 bp, and 3311 bp, consistent with the predicted digestion pattern and validating the precise integration of the CD22-scFv gene into the pET-28a(+) expression vector. Lane assignments: 1-kbp DNA ladder (Lane 1), undigested recombinant clone control (Lane 2), and *PvuII*-digested recombinant plasmid (Lane 3). (D) The schematic diagram of the CD22-scFv-pET28a+ plasmid was constructed for CD22-scFv expression in *Escherichia coli.* The restriction enzyme sites of *Xho*I, *Bam*HI, and *Pvu*II are indicated. scFv, Single-chain variable fragment.

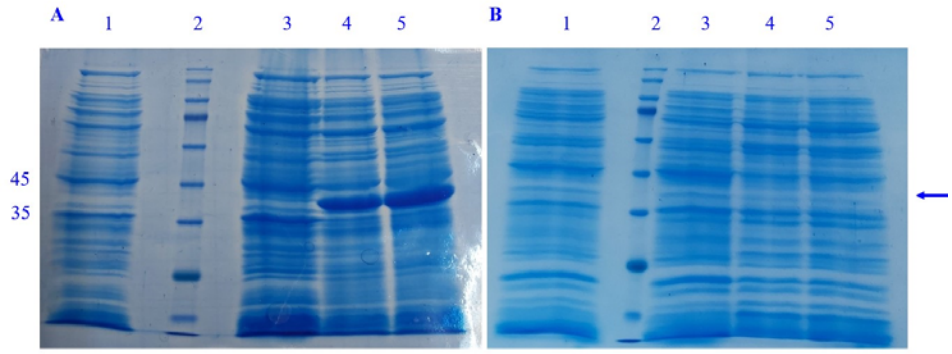

Fig. 3. Expression analysis of CD22-scFv in *Escherichia coli* host strains by SDS-PAGE. (A) SDS-PAGE analysis of CD22-scFv expression in Rosetta (DE3) cells. Lane assignments: negative control (cells without the expression plasmid, Lane 1), protein marker (Lane 2), uninduced sample (cells before induction, Lane 3), and two independent clones induced with 1 mM IPTG for 18 h (Lanes 4 and 5), showing a distinct band at approximately 38 kDa, indicative of CD22-scFv expression. (B) SDS-PAGE analysis of CD22-scFv expression in Rosetta-gami-2 cells. Lane assignments: negative control (cells without the expression plasmid, Lane 1), protein marker (Lane 2), uninduced sample (cells before induction, Lane 3), and two independent clones induced with 1 mM IPTG for 18 h (Lanes 4 and 5). No band at ~38 kDa was detected. scFv, Single-chain variable fragment; SDS-PAGE, sodium dodecyl-sulfate polyacrylamide gel electrophoresis; IPTG, isopropyl β-D-1-thiogalactopyranoside.

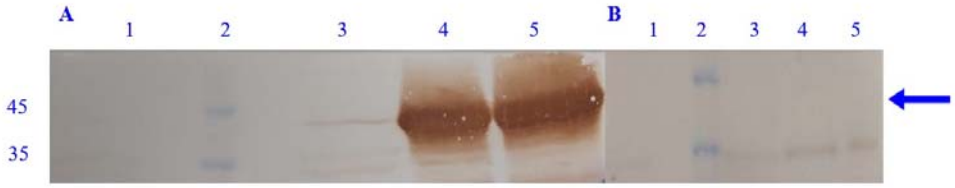

Fig. 4. Western blot analysis of CD22-scFv expression in *Escherichia coli* host strains. (A) Western blot analysis of CD22-scFv expression in Rosetta (DE3) cells. Lane assignments: negative control (cells without the expression plasmid, Lane 1), protein marker (Lane 2), uninduced sample (cells before induction, Lane 3), and two independent clones induced with 1 mM IPTG for 18 h (Lanes 4 and 5), each displaying a prominent band at approximately 38 kDa, corresponding to CD22-scFv. (B) Western blot analysis of CD22-scFv expression in Rosetta-gami-2 cells. Lane assignments: negative control (cells without the expression plasmid, Lane 1), protein marker (Lane 2), uninduced sample (cells before induction, Lane 3), and two independent clones induced with 1 mM IPTG for 18 h(Lanes 4 and 5). No CD22-scFv expression was recorded. scFv, Single-chain variable fragment; IPTG, isopropyl β-D-1-thiogalactopyranoside.

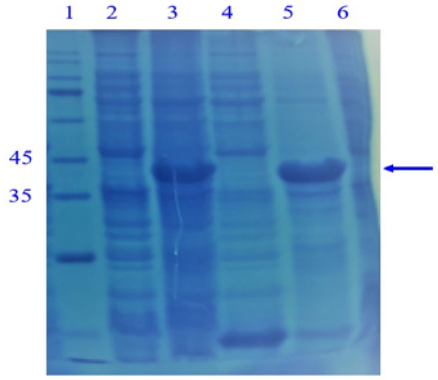

Fig. 5. SDS-PAGE analysis of CD22-scFv solubility in Rosetta (DE3) cells. Lane assignments: protein marker (Lane 1); expression host control - Rosetta (DE3) without pET-28a(+)-CD22-scFv, negative control (Lane 2); induced control - total protein from Rosetta (DE3) containing pET-28a(+)-CD22-scFv after IPTG induction, showing total expression level (including both soluble and insoluble forms) (Lane 3); crude extract A - soluble fraction (supernatant after sonication and centrifugation, (Lane 4); crude extract B - insoluble fraction (pellet after centrifugation, Lane 5); Rosetta (DE3) containing pET-28a(+)-CD22-scFv before IPTG induction, non-induced control (Lane 6). The predominant presence of CD22-scFv in the insoluble fraction (Lane 5) indicates that under the tested conditions, the majority of expressed CD22-scFv forms inclusion bodies. scFv, Single-chain variable fragment; SDS-PAGE, sodium dodecyl-sulfate polyacrylamide gel electrophoresis; IPTG, isopropyl β-D-1-thiogalactopyranoside.

Purification of CD22-scFv under hybrid conditions

SDS-PAGE analysis of elution fractions revealed a distinct band at approximately 38 kDa (Fig. 6, Lanes 6-8), consistent with the expected molecular weight of CD22-scFv. The absence of significant protein bands in the flow-through and wash fractions confirmed efficient binding of CD22-scFv to the Ni-NTA resin and effective removal of non-specifically bound proteins. These results demonstrate the successful expression and purification of CD22-scFv under optimized hybrid conditions, ensuring high purity and recovery of the target protein.

Effects of IPTG concentration on the expression of soluble fraction of CD22-scFv

As shown in Fig. 7, SDS-PAGE analysis of soluble (crude sample A) and insoluble (crude sample B) fractions revealed faint bands corresponding to CD22-scFv in crude sample A at IPTG concentrations of 0.2, 0.5, and 0.75 mM (Fig. 7, Lanes 7, 9, and 11), indicating limited soluble protein production. In contrast, broader and more intense bands were observed in crude sample B across all IPTG concentrations (Fig. 7, Lanes 4, 6, 8, 10, 12, and 14), suggesting that the majority of the expressed protein was insoluble. Based on these observations, 0.5 mM IPTG was selected for further optimization due to the relatively more distinct band in the soluble fraction.

Effects of post-induction temperature and time on CD22-scFv protein solubility

SDS-PAGE analysis (Fig. 8A-C) revealed that lower temperatures, particularly 25 °C, significantly enhanced soluble-protein yield compared to higher temperatures. An incubation period of 8 h at 25 °C resulted in the highest proportion of soluble CD22-scFv, while prolonged induction (18 h) reduced solubility.

Purification of CD22-scFv under native conditions

SDS-PAGE analysis of the elution fractions revealed a distinct band at approximately 38 kDa (Fig. 9, Lanes 6-8), corresponding to the expected molecular weight of CD22-scFv, confirming successful purification of the target protein under native conditions using Ni-NTA affinity chromatography.

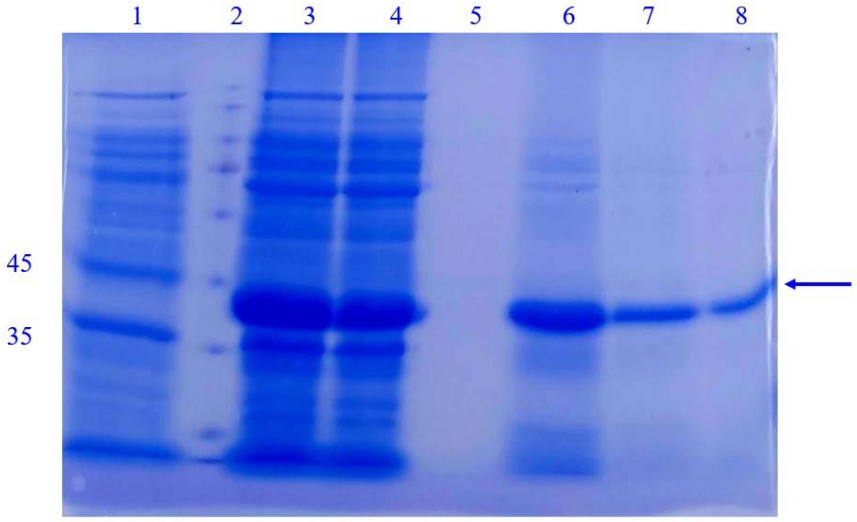

Fig. 6. SDS-PAGE analysis of CD22-scFv purification under hybrid conditions. Lane assignments: negative control cells without the expression plasmid, (Lane 1); protein marker (Lane 2); crude lysate containing total expressed proteins (Lane 3); flow-through fraction, representing unbound proteins (Lane 4); wash 5 fraction (washing buffer 3, Table S2), ensuring the removal of non-specifically bound proteins (Lane 5); elution fractions of 3, 4, and 5 (elution buffer 2, Table S2), containing the purified CD22-scFv protein (Lanes 6-8). The distinct band at approximately 38 kDa in the elution fractions (Lanes 6-8) confirms the successful purification of CD22-scFv under hybrid conditions. scFv, Single-chain variable fragment; SDS-PAGE, sodium dodecyl-sulfate polyacrylamide gel electrophoresis.

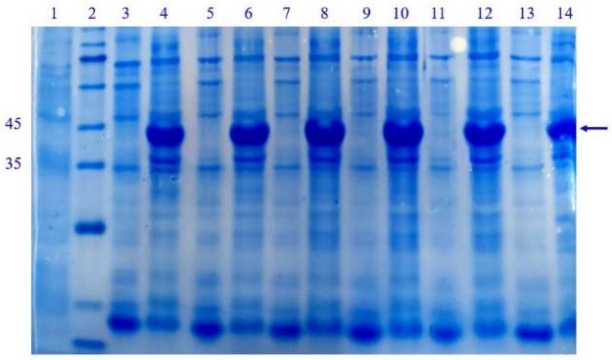

Fig. 7. SDS-PAGE analysis of CD22-scFv expression under varying IPTG concentrations. Lane 1 serves as the negative control, consisting of Rosetta (DE3) cells without the expression plasmid; Lane 2 contains a protein molecular weight marker. Lanes 3, 5, 7, 9, 11, and 13 represent the soluble fractions (crude extract A) from cells induced with IPTG concentrations of 0.05, 0.1, 0.2, 0.5, 0.75, and 1 mM, respectively. The corresponding insoluble fractions (crude extract B) under identical conditions are shown in Lanes 4, 6, 8, 10, 12, and 14. The analysis indicates that a distinct band at approximately 38 kDa, corresponding to CD22-scFv, is predominantly observed in the soluble fractions induced with IPTG at 0.5 mM, with a lesser extent of expression at 0.75 mM. In contrast, the insoluble fractions exhibit broad protein expression across all tested IPTG concentrations. These findings suggest that 0.5 mM IPTG is the optimal concentration for further optimization of CD22-scFv protein expression. scFv, Single-chain variable fragment; SDS-PAGE, sodium dodecyl-sulfate polyacrylamide gel electrophoresis; IPTG, isopropyl β-D-1-thiogalactopyranoside.

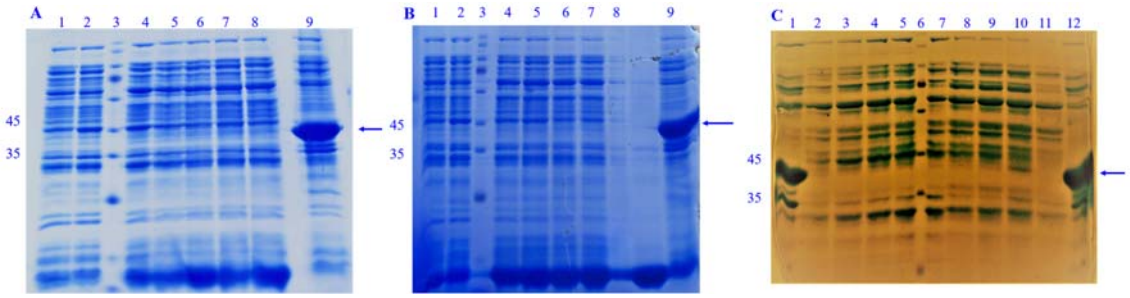

Fig. 8. Optimization of post-induction temperature and time for CD22-scFv solubility. (A) Optimization of post-induction time at 25 °C: Lane 1 represents the non-induced control, while Lane 2 serves as the negative control, consisting of bacteria without the expression plasmid. Lane 3 contains a protein marker. Lanes 4-8 correspond to the soluble fractions (crude extract A) after induction for 2, 4, 6, 8, and 18 h, respectively. Lane 9 shows the insoluble fraction (crude extract B) after 18 h post-induction. (B) Optimization of post-induction temperature at 30 °C: Lane 1 is the non-induced control, and Lane 2 is the negative control, similar to part A. Lane 3 contains a protein marker. Lanes 4-8 represent the soluble fractions (crude extract A) after induction for 2, 4, 6, 8, and 18 h, respectively. Lane 9 corresponds to the insoluble fraction (crude extract B) after 18 h post-induction. (C) Comparison of post-induction times at 20 °C and 37 °C: At 20 °C, Lanes 1 and 2-5 represent the insoluble fraction after 18 h and the soluble fractions after 18, 8, 6, and 4 h, respectively. Lane 6 contains a protein marker, and Lane 7 is the negative control (cells without the expression plasmid). At 37 °C, Lanes 8-11 correspond to the soluble fractions (crude extract A) after induction for 4, 6, 8, and 18 h, respectively, with Lane 12 showing the insoluble fraction (crude extract B) after 18 h post-induction. The analysis reveals the optimal conditions for enhancing the solubility of CD22-scFv by adjusting post-induction temperature and time, which is crucial for improving protein functionality and yield. These findings are consistent with the importance of optimizing expression conditions for recombinant proteins, as seen in similar studies involving anti-CD22 scFv constructs. scFv, Single-chain variable fragment.

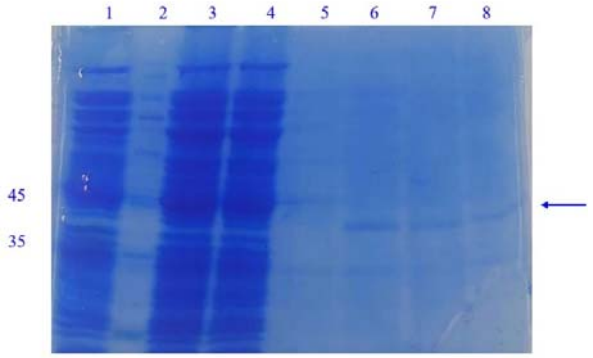

Fig. 9. Purification of CD22-scFv under native conditions. Lane 1 represents the negative control, consisting of bacteria without the expression plasmid; Lane 2 contains a protein molecular weight marker. Lane 3 shows the crude lysate containing the total expressed proteins. Lane 4 corresponds to the flow-through fraction, which includes unbound proteins. Lane 5 represents the wash fraction (using washing buffer 2, as detailed in Table S1), ensuring the removal of non-specifically bound proteins. Lanes 6-8 are the elution fractions of 2, 3, and 4 (using elution buffers 1 and 2, as detailed in Table S1), demonstrating the purified CD22-scFv protein. A distinct band at approximately 38 kDa in the elution fractions confirms the successful purification of CD22-scFv under native conditions. scFv, Single-chain variable fragment.

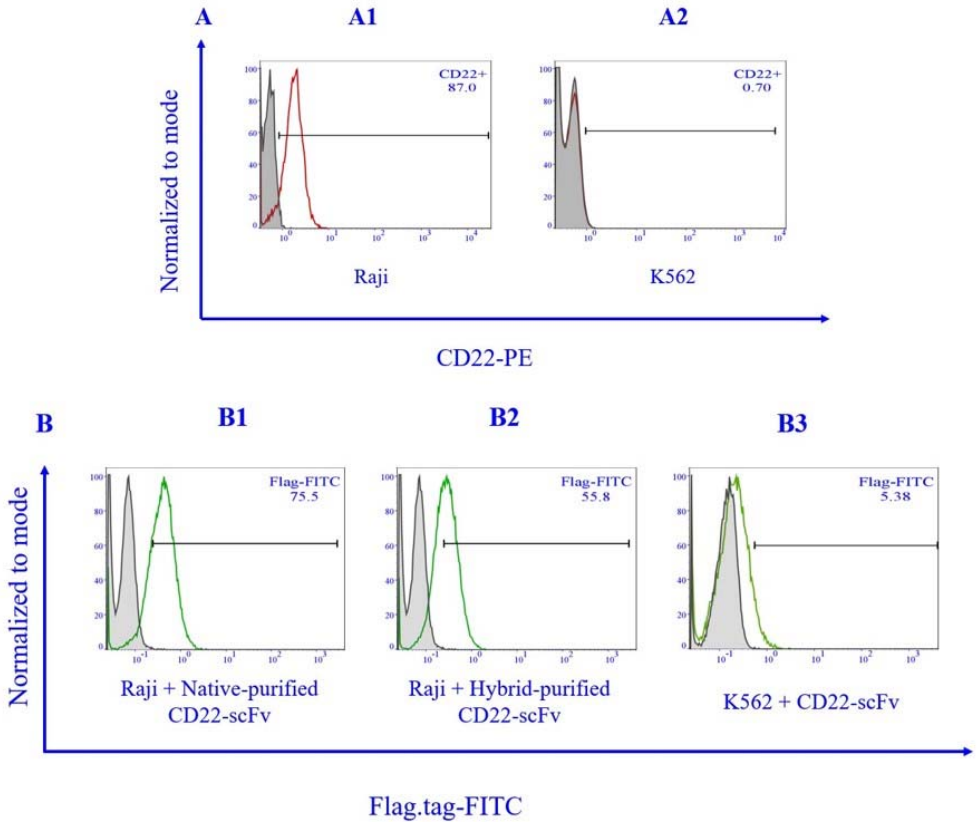

Fig. 10. Flow cytometry analysis of CD22 expression and CD22-scFv binding. The flow cytometry analysis of CD22 surface expression and the binding of CD22-scFv to Raji and K562 cells. (A) Flow cytometry analysis of CD22 surface expression on Raji and K562 cells using a commercial monoclonal anti-CD22 antibody revealed that (A1) 87% of Raji cells expressed CD22, while (A2) K562 cells showed minimal expression (0.7%). (B) Flow cytometry analysis of CD22-scFv binding to Raji ($CD22^+$) and K562 ($CD22^-$) cells using anti-FLAG primary and FITC-conjugated secondary antibodies. (B1) The native-purified CD22-scFv demonstrated a binding efficiency of 75.5% to Raji cells, whereas (B2) the hybrid-purified CD22-scFv showed a binding efficiency of 55.8%. A pronounced fluorescence shift in Raji cells indicated strong CD22-scFv binding, while (B3) K562 cells displayed negligible fluorescence, confirming the specificity of CD22-scFv for CD22-expressing cells. scFv, Single-chain variable fragment; PE, phycoerythrin; FITC, fluorescein isothiocyanate.

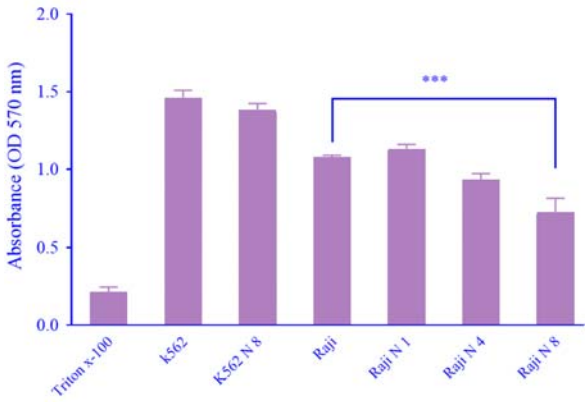

Fig. 11. Evaluation of the proliferation of Raji Cells. The proliferation of Raji cells was assessed using the MTT assay to evaluate the impact of CD22-scFv on cell growth. The results indicate that native-purified CD22-scFv at 8 µg/mL significantly reduces the proliferation of CD22-positive Raji cells. In contrast, CD22-negative K562 cells were unaffected by CD22-scFv treatment. This differential effect highlights the specificity of CD22-scFv for CD22-expressing cells, supporting its potential as a targeted therapeutic agent. scFv, Single-chain variable fragment.

Flow cytometry analysis of CD22 expression and CD22-scFv binding

The analysis revealed that 87% of Raji cells were positive for CD22, however, K562 cells showed no detectable CD22 expression (Fig. 10A). Additionally, flow cytometry demonstrated that both native-purified and hybrid-purified CD22-scFv molecules recognized the CD22 antigen on Raji cells, resulting in a fluorescence intensity shift compared to K562 cells. The binding efficiency of native-purified CD22-scFv was 75.5%, higher than the 55.8% observed for hybrid-purified CD22-scFv (Fig. 10B). These findings confirm the selective binding of CD22-scFv to CD22-expressing cells, with native-purified CD22-scFv exhibiting enhanced binding efficiency.

Analysis of Raji cells' proliferation

The MTT assay evaluated the proliferation of Raji cells in the presence of native-purified CD22-scFv. The results showed that CD22-scFv at 8 µg/mL significantly decreased the proliferation of $CD22^+$ Raji cells, while it did not affect CD22- K562 cells (Fig. 11).

DISCUSSION

Targeted therapies have revolutionized cancer treatment by significantly improving overall survival while minimizing side effects. Among these, mAbs have emerged as a leading form of targeted therapy due to their ability to effectively inhibit cancer cell proliferation and eliminate malignant cells (27). The success of mAbs can be attributed to several key advantages, including their prolonged serum half-life, heightened affinity, exceptional specificity, and capacity to exert immune effector functions (28). These properties have enabled mAbs to make significant progress in the treatment of lymphoid and myeloid hematological malignancies (29,30). Despite their promise, mAbs also face notable therapeutic limitations. The large size of these proteins (~150 kDa) requires complex post-translational modifications, necessitating mammalian cell cultures and extensive purification under good manufacturing practice standards. This results in high production costs and lengthy manufacturing times, limiting the widespread therapeutic application of mAbs (31-33). Additionally, the large size of mAbs prevents them from being filtered by the kidneys and excreted in the urine (34). Moreover, mAbs' efficacy can be diminished by competition with endogenous IgGs for Fcγ receptors, inhibitory receptors like FcγRIIb, and patient-specific FcγR polymorphisms (33).

The genetic engineering has led to the development of diverse antibody formats to address these limitations. For instance, scFvs, created by modifying or removing the Fc region, can retain the antigen-binding specificity of full-length antibodies while overcoming several of their drawbacks (35). The compact structure of scFvs offers distinct advantages in cancer treatment and biomarker research. Their smaller size allows for better tissue penetration, while their mono- and multi-specificity, superior tissue retention, and improved functional affinity enhance their therapeutic potential (36). Moreover, the absence of the Fc region eliminates unwanted immune responses and competition with endogenous antibodies, addressing key

limitations of full-length mAbs. Production of scFvs has been optimized by cloning of immunoglobulin genes, enabling expression in both prokaryotic and eukaryotic systems. This approach enhances reproducibility, reduces costs, and accelerates production timelines compared to traditional mAb manufacturing (37,38). Among these systems, *E. coli* has emerged as an attractive option for scFv production due to its simplicity, rapid growth, and cost-effectiveness. The absence of glycosylation in scFv fragments further simplifies their production in *E. coli* (39). However, *E. coli* expression systems present challenges, particularly in producing functional scFvs with correct disulfide bonds. Overexpression of scFv proteins in the *E. coli* cytoplasm often results in misfolding and formation of insoluble aggregates, leading to non-functional proteins (39). To mitigate this, researchers have focused on optimizing the reduction-oxidation pathways in *E. coli*. Specifically, strains like Origami, which are trxB and gor mutants, have been developed to facilitate improved folding of disulfide-containing proteins (40-42), such as antibody fragments in the *E. coli* cytoplasm (39). These advancements in *E. coli* engineering are crucial for the efficient production of bioactive scFvs, further enhancing their potential as a next-generation therapeutic tool in cancer treatment.

Rosetta (DE3) strains, derived from BL21, have been engineered to improve the expression of proteins containing codons infrequently found in *E. coli* (43). Rosetta-gami-2, a combination of Origami 2 and Rosetta 2, enhances disulfide bond formation and rare codon translation (44). Based on the presence of eukaryotic codons and disulfide bonds in CD22-scFv, we employed Rosetta (DE3) and Rosetta-gami-2 for expression. Our results, as revealed by Western blot (Fig. 4) and SDS-PAGE (Fig. 3), showed higher CD22-scFv production in Rosetta (DE3). This finding is consistent with the results reported by Shafiee *et al*., demonstrating superior expression in Rosetta (DE3) compared to BL21 (DE3) and Rosetta-gami-2 (45).

We utilized a cost-effective and efficient IMAC-based one-step method for protein purification using imidazole and urea. IMAC is widely applied for purifying recombinant proteins due to its simplicity and versatility under denaturing and native conditions. This method allows for on-column refolding, ensuring high affinity and specificity (23,24). Previous studies have demonstrated that simultaneous purification and refolding in one IMAC step can be time-efficient, cost-effective, and yield higher protein concentrations. Esfandiar *et al.* achieved 97% purity with comparable activity to commercial interleukin-2 by purifying native and active interleukin-2 from IBs using a gradient of urea and imidazole during washing and elution (25). Similarly, Ahmadzadeh *et al.* purified the IP-10-(anti-HER2 scFv) fusion protein with 96% purity and a 15% recovery yield using a comparable approach (46). Akbari *et al.* compared native, denaturing, and hybrid conditions for anti-HER2-scFv purification using Ni-NTA affinity chromatography, finding that denaturing conditions yielded higher results than native conditions, which in turn outperformed hybrid conditions (47). Notably, these results differed from those reported by Ahmadzadeh *et al*., highlighting the variability in outcomes when using similar purification approaches (46). This simultaneous purification and refolding approach using IMAC offers an efficient, cost-effective method for protein purification, minimizing loss while preserving structure and function. Moreover, it is scalable for large-scale production, simplifying processes and reducing reagent use.

Although CD22-scFv expression in Rosetta (DE3) cells was high, solubility tests revealed that the protein was primarily in the form of IBs. Optimizing environmental factors such as expression strain, post-induction temperature, induction time, and IPTG concentration is essential for improving the solubility of recombinant proteins, as improper expression conditions often lead to misfolding and aggregation into IBs (21). Studies have shown that higher concentrations of IPTG can have toxic effects on the host by reducing the rate of cell growth and increasing the expression rate of low-quality proteins in the form of IBs (48,49). In the present study, IPTG concentrations ranging from 0.05 to 1 mM were tested for CD22-scFv-pET-28a(+) expression

in Rosetta (DE3). The highest solubility was achieved with 0.5 mM IPTG (Fig. 7), consistent with other findings showing that lower IPTG concentrations enhance recombinant protein solubility in BL21 (DE3) (50,51), BL21 (DE3) pLysS (51), Rosetta (DE3) (52), Origami (DE3) (50), and SHuffle® T7 (15). Protein accumulation is accelerated at higher temperatures due to enhanced hydrophobic interactions. Overexpression, often achieved through strong promoters and high inducer concentrations during the mid-log phase (OD_{600} 0.6-0.8), can lead to protein aggregation. Lowering the temperature mitigates the activation of heat shock proteases triggered by overexpression, thereby reducing the aggregation of both folded and misfolded proteins (41,53). Factors such as limited cytosolic space, the absence of PTMs, and decreased activity of *E. coli* chaperones at temperatures above 30°C contribute to the formation of IBs (54). These conditions promote protein aggregation, impacting their quality and solubility. Interestingly, *E. coli* grown at lower temperatures (25 °C) produces non-classical IBs with native-like secondary structures (16,17,55). Our study examined the effect of post-induction temperatures (20-37 °C) on the solubility of CD22-scFv in Rosetta (DE3). We observed that lowering the temperature increased solubility, with the highest rate at 25 °C (Fig. 8A). This finding aligns with previous studies demonstrating that reducing induction temperatures improves the soluble-to-insoluble protein ratio, with optimal results often reported at 25 °C across various strains (46). Similar improvements in solubility have been noted in other proteins. Koçer *et al.* reported a three-fold increase in soluble scFv-VLVH when the temperature was reduced from 30 °C to 16 °C (56). Enhanced soluble production of GM-CSF at 30 °C in SHuffle® T7 *E. coli* strains (15), and improved productivity of a recombinant epithelial cell adhesion molecule extracellular domain fusion protein at 16 °C with reduced IPTG concentration (53). Collectively, these studies confirm that lower cultivation temperatures enhance protein solubility and stability by preventing aggregation (57). Our results culminated in a final yield of 15.86 mg/L for hybrid-purified CD22-scFv and 3.65 mg/L for native-purified CD22-scFv.

We utilized the *E. coli* expression system for CD22-scFv production due to its cost-effectiveness, rapid growth, and ease of process optimization, making it particularly suitable for small antibody fragments like scFv. In contrast, yeast systems such as *Pichia pastoris* offer eukaryotic PTMs and high yields but require longer cultivation times and higher costs. Similarly, mammalian systems like Chinese hamster ovary cells provide authentic PTMs and proper folding, but are less practical for scFv production due to slower growth rates and higher operational expenses. Despite *E. coli's* limitations, including IBs formation and the absence of eukaryotic PTMs, our systematic optimization significantly improved CD22-scFv solubility and yield. Furthermore, implementing a cost-effective hybrid IMAC-based on-column refolding purification strategy supports *E. coli* as a practical choice for scalable production, especially for preclinical and early therapeutic applications (58).

While our purification strategy is efficient at the laboratory scale, transitioning to large-scale industrial production poses several challenges. Key factors such as fermentation conditions, endotoxin removal, and process robustness must be optimized to ensure batch-to-batch consistency. Additionally, the economic feasibility of scaling up *E. coli*-based production needs to be assessed in comparison to alternative platforms. Future studies should focus on optimizing bioreactor parameters, refining purification protocols, and implementing good manufacturing practice standards to facilitate clinical translation.

We analyzed the interaction of CD22-scFv, purified under native or hybrid conditions, with $CD22^+$ Raji cells using flow cytometry. CD22-scFv demonstrated significant binding to $CD22^+$ Raji cells, with 75.5% binding for native-purified and 55.8% for hybrid-purified CD22-scFv, while no binding was observed with $CD22^-$ K562 cells (Fig. 10B). Zarei *et al.* previously showed that CD22-scFv (humanized RFB4), expressed in *Pichia pastoris*, preferentially binds to $CD22^+$-expressing cell lines, indicated by a fluorescence shift in $CD22^+$ Raji cells and lower fluorescence intensity in $CD22^-$ Jurkat cells (59). Similarly, Mikiewicz *et al.* provided evidence that anti-

CD22-scFv, purified using the SP Sepharose fast flow column, specifically binds to $CD22^+$ Raji and Daudi cells but not to $CD22^-$ K562 cells (10). These findings collectively validate the specificity of CD22-scFv for CD22-expressing cells and highlight its potential in targeted therapies.

We hypothesized that CD22-scFv binding to Raji cells could inhibit their proliferation. The MTT assay revealed that 8 µg/mL of native-purified CD22-scFv significantly reduced the proliferation of $CD22^+$ Raji cells without affecting $CD22^-$ K562 cells (Fig. 11). While the anti-proliferative effects of CD22-scFv were evident in our *in vitro* assays, the precise molecular mechanisms underlying these effects remain to be fully elucidated. We propose two potential pathways: CD22-scFv binding may induce an inhibitory signaling cascade *via* CD22-associated proteins such as SHP-1, leading to reduced proliferation; or CD22-scFv may sterically hinder essential interactions for cell survival and proliferation. Previous studies have demonstrated that CD22 recruits SHP-1 to attenuate BCR signaling and regulate cell cycle progression. Additionally, as an adhesion molecule, interactions of CD22 with ligands play a critical role in maintaining B-cell homeostasis (60). However, the proposed mechanisms remain speculative in the absence of direct experimental validation, which constitutes a limitation of this study. Future research should focus on targeted signaling analyses, such as phospho-protein profiling and transcriptomic approaches, to elucidate the downstream molecular effects of CD22-scFv engagement. Advanced methodologies, including western blotting for phosphorylated signaling intermediates and RNA sequencing, could provide critical insights into the mechanistic underpinnings of the anti-proliferative activity of CD22-scFv, thereby reinforcing its therapeutic potential. While the *in vitro* results are promising, the lack of *in vivo* validation represents another notable limitation of this work. To address this, preliminary *in vivo* studies using appropriate animal models, such as xenograft models of $CD22^+$ B-cell malignancies, should be conducted. These investigations will be essential for evaluating key parameters, including pharmacokinetics, biodistribution, immunogenicity, and therapeutic efficacy of CD22-scFv. Additionally, they will allow for the assessment of potential off-target effects and immune responses and critical considerations for clinical translation. These efforts will not only enhance the clinical relevance of our findings but also facilitate the advancement of CD22-scFv toward therapeutic applications.

CONCLUSION

This study presents a transformative framework for the scalable and cost-effective production of CD22-scFv, effectively addressing key challenges associated with recombinant antibody fragment expression in *E. coli*. Through the optimization of critical parameters and the implementation of innovative purification strategies, we have successfully produced functional CD22-scFv with high specificity and potent anti-proliferative activity against $CD22^+$ tumor cells. These advancements address the pressing need for accessible and precise biotherapeutics, particularly in B-cell malignancies. Beyond its standalone therapeutic potential, CD22-scFv shows promise as a foundational component for advanced cell-based therapies, including CAR-T and CAR-NK cell platforms, which are revolutionizing precision oncology. This work establishes a foundation for integrating recombinant scFvs into next-generation immunotherapies, enhancing their efficacy and scalability for clinical applications. By bridging existing gaps in therapeutic modalities, this approach represents a critical step toward developing personalized, accessible, and impactful cancer treatments.

Acknowledgments

This study was funded by Tabriz University of Medical Sciences (Ph.D. thesis grant to Monireh Gholizadeh, Grant No. 61571) and the National Institute for Medical Research Development (NIMAD) through Grant No. 4000399.

We sincerely thank the Pasteur Institute of Iran for technical support and valuable resources during this study. Their participation was instrumental in the successful completion of this research.

Conflict of interest statement

The authors declared no conflict of interest in this study.

Contributors' contributions

Z. Sharifzadeh and Sh. Abdoli contributed to the conception and design of the study. M. Gholizadeh and Sh. Mansoori performed the experimental work. Z. Sharifzadeh, F. Riazi-Rad, and A. Arashkia were responsible for data analysis. M. Gholizadeh, Z. Sharifzadeh, A. Ali Hamidieh, and M. Nouri were responsible for writing, editing, and reviewing the manuscript. The finalized article was read and approved by all authors.

Ethics approval

All experiments have been conducted according to the guidelines of the Ethics Committee of Tabriz University of Medical Sciences, IR.TBZMED.REC.1397.974.

REFERENCES

1. Keykhaei M, Masinaei M, Mohammadi E, Azadnajafabad S, Rezaei N, Saeedi Moghaddam S, *et al*. A global, regional, and national survey on burden and quality of care index (QCI) of hematologic malignancies; global burden of disease systematic analysis 1990–2017. Exp Hematol Oncol. 2021;10(1):11,1-15. DOI: 10.1186/s40164-021-00198-2.
2. Zhang N, Wu J, Wang Q, Liang Y, Li X, Chen G, *et al*. Global burden of hematologic malignancies and evolution patterns over the past 30 years. Blood Cancer J. 2023;13(1):1-13. DOI: 10.1038/s41408-023-00853-3.
3. Sullivan-Chang L, O'Donnell RT, Tuscano JM. Targeting CD22 in B-cell malignancies: current status and clinical outlook. BioDrugs. 2013;27(4):293-304. DOI: 10.1007/s40259-013-0016-7.
4. Zawada JF, Yin G, Steiner AR, Yang J, Naresh A, Roy SM, *et al*. Microscale to manufacturing scale-up of cell-free cytokine production- a new approach for shortening protein production development timelines. Biotechnol Bioeng. 2011;108(7):1570-1578. DOI: 10.1002/bit.23103.
5. Kesik-Brodacka M. Progress in biopharmaceutical development. Biotechnol Appl Biochem. 2018;65(3):306-322. DOI: 10.1002/bab.1617.
6. Rader RA. (Re)defining biopharmaceutical. Nat Biotechnol. 2008;26(7):743-751. DOI: 10.1038/nbt0708-743.
7. Li W, Prabakaran P, Chen W, Zhu Z, Feng Y, Dimitrov DS. Antibody aggregation: insights from sequence and structure. Antibodies. 2016;5(3): 19,1-23. DOI: 10.3390/antib5030019.
8. Vázquez-Rey M, Lang DA. Aggregates in monoclonal antibody manufacturing processes. Biotechnol Bioeng. 2011;108(7):1494-1508. DOI: 10.1002/bit.23155.
9. Edwards E, Livanos M, Krueger A, Dell A, Haslam SM, Mark Smales C, *et al*. Strategies to control therapeutic antibody glycosylation during bioprocessing: synthesis and separation. Biotechnol Bioeng. 2022;119(6):1343-1358. DOI: 10.1002/bit.28066.
10. Mikiewicz D, Łukasiewicz N, Zieliński M, Cecuda-Adamczewska V, Bierczyńska-Krzysik A, Romanik-Chruścielewska A, *et al*. Bacterial expression and characterization of an anti-CD22 single-chain antibody fragment. Protein Expr Purif. 2020;170:105594,1-8. DOI: 10.1016/j.pep.2020.105594.
11. Holliger P, Hudson PJ. Engineered antibody fragments and the rise of single domains. Nat Biotechnol. 2005;23(9):1126-1136. DOI: 10.1038/nbt1142.
12. Gupta V, Sudhakaran IP, Islam Z, Vaikath NN, Hmila I, Lukacsovich T, *et al*. Expression, purification and characterization of α-synuclein fibrillar specific scFv from inclusion bodies. PLoS One. 2020;15(11):1-17. DOI: 10.1371/journal.pone.0241773.
13. Tripathi NK, Shrivastava A. Recent developments in bioprocessing of recombinant proteins: expression hosts and process development. Front Bioeng Biotechnol. 2019;7:420,1-35. DOI: 10.3389/fbioe.2019.00420.
14. Gholizadeh M, Khanahmad H, Memarnejadian A, Aghasadeghi MR, Roohvand F, Sadat SM, *et al*. Design and expression of fusion protein consists of HBsAg and Polyepitope of HCV as an HCV potential vaccine. Adv Biomed Res. 2015;4:243,1-7. DOI: 10.4103/2277-9175.168610.
15. Soheili S, Jahanian-Najafabadi A, Akbari V. Evaluation of soluble expression of recombinant granulocyte macrophage stimulating factor (rGM-CSF) by three different *E. coli* strains. Res Pharm Sci. 2020;15(3):218-225. DOI: 10.4103/1735-5362.288424.
16. Jevševar S, Gaberc-Porekar V, Fonda I, Podobnik B, Grdadolnik J, Menart V. Production of nonclassical inclusion bodies from which correctly folded protein can be extracted. Biotechnol Prog. 2005;21(2): 632-639. DOI: 10.1021/bp0497839.
17. Ventura S, Villaverde A. Protein quality in bacterial inclusion bodies. Trends Biotechnol. 2006;24(4):179-185. DOI: 10.1016/j.tibtech.2006.02.007.
18. Zhu S, Gong C, Ren L, Li X, Song D, Zheng G. A simple and effective strategy for solving the problem of inclusion bodies in recombinant protein technology: His-tag deletions enhance soluble expression. Appl Microbiol Biotechnol. 2013;97(2):837-845. DOI: 10.1007/s00253-012-4630-y.

19. Gutiérrez-González M, Farías C, Tello S, Pérez-Etcheverry D, Romero A, Zúñiga R, *et al.* Optimization of culture conditions for the expression of three different insoluble proteins in *Escherichia coli*. Sci Rep. 2019;9(1):16850,1-11. DOI: 10.1038/s41598-019-53200-7.
20. Song HN, Jang JH, Kim YW, Kim DH, Park SG, Lee MK, *et al*. Refolded scFv antibody fragment against myoglobin shows rapid reaction kinetics. Int J Mol Sci. 2014;15(12):23658-23671. DOI: 10.3390/ijms151223658.
21. San-Miguel T, Pérez-Bermúdez P, Gavidia I. Production of soluble eukaryotic recombinant proteins in *E. coli* is favoured in early log-phase cultures induced at low temperature. Springerplus. 2013;2(1):89,1-4. DOI: 10.1186/2193-1801-2-89.
22. Bhatwa A, Wang W, Hassan YI, Abraham N, Li XZ, Zhou T. Challenges associated with the formation of recombinant protein inclusion bodies in *Escherichia coli* and strategies to address them for industrial applications. Front Bioeng Biotechnol. 2021;9:630551,1-18. DOI: 10.3389/fbioe.2021.630551.
23. Glynou K, Ioannou PC, Christopoulos TK. One-step purification and refolding of recombinant photoprotein aequorin by immobilized metal-ion affinity chromatography. Protein Expr Purif. 2003;27(2):384-390. DOI: 10.1016/S1046-5928(02)00614-9.
24. Block H, Maertens B, Spriestersbach A, Brinker N, Kubicek J, Fabis R, *et al*. Immobilized-Metal Affinity Chromatography (IMAC). Methods Enzymol. 2009;463:439-473. DOI: 10.1016/S0076-6879(09)63027-5.
25. Esfandiar S, Hashemi-Najafabadi S, Shojaosadati SA, Sarrafzadeh SA, Pourpak Z. Purification and refolding of *Escherichia coli-expressed* recombinant human interleukin-2. Biotechnol Appl Biochem. 2010;55(4):209-214. DOI: 10.1042/BA20090256.
26. Liu M, Wang X, Yin C, Zhang Z, Lin Q, Zhen Y, *et al*. One-step on-column purification and refolding of a single-chain variable fragment (scFv) antibody against tumour necrosis factor α. Biotechnol Appl Biochem. 2006;43(3):137-145. DOI: 10.1042/BA20050194.
27. Jin S, Sun Y, Liang X, Gu X, Ning J, Xu Y, *et al*. Emerging new therapeutic antibody derivatives for cancer treatment. Signal Transduct Target Ther. 2022;7(1):39,1-28. DOI: 10.1038/s41392-021-00868-x.
28. Zinn S, Vazquez-Lombardi R, Zimmermann C, Sapra P, Jermutus L, Christ D. Advances in antibody-based therapy in oncology. Nat Cancer. 2023;4(2):165-180. DOI: 10.1038/s43018-023-00516-z.
29. Wayne AS, FitzGerald DJ, Kreitman RJ, Pastan I. Immunotoxins for leukemia. Blood. 2014;123(16):2470-2477. DOI: 10.1182/blood-2014-01-492256.
30. Tu X, LaVallee T, Lechleider R. CD22 as a target for cancer therapy. J Exp Ther Oncol. 2011;9(3): 241-248. PMID: 22070056.
31. Wallace ZS, Harkness T, Blumenthal KG, Choi HK, Stone JH, Walensky RP. Increasing operational capacity and reducing costs of rituximab administration: a costing analysis. ACR Open Rheumatol. 2020;2(5):261-268. DOI: 10.1002/acr2.11133.
32. Kholodenko RV, Kalinovsky DV, Doronin II, Ponomarev ED, Kholodenko IV. Antibody fragments as potential biopharmaceuticals for cancer therapy: success and limitations. Curr Med Chem. 2019;26(3):396-426. DOI: 10.2174/0929867324666170817152554.
33. Chames P, Van Regenmortel M, Weiss E, Baty D. Therapeutic antibodies: successes, limitations and hopes for the future. Br J Pharmacol. 2009;157(2):220-233. DOI: 10.1111/j.1476-5381.2009.00190.x.
34. Ryman JT, Meibohm B. Pharmacokinetics of monoclonal antibodies. CPT Pharmacomet Syst Pharmacol. 2017;6(9):576-588. DOI: 10.1002/psp4.12224.
35. Rodríguez-Nava C, Ortuño-Pineda C, Illades-Aguiar B, Flores-Alfaro E, Leyva-Vázquez MA, Parra-Rojas I, *et al*. Mechanisms of action and limitations of monoclonal antibodies and single chain fragment variable (scFv) in the treatment of cancer. Biomedicines. 2023;11(6):1610,1-25. DOI: 10.3390/biomedicines11061610.
36. Brofelth M, Städe LW, Ekstrand AI, Edfeldt LP, Kovačič R, Nielsen TT, *et al*. Site-specific photocoupling of pBpa mutated scFv antibodies for use in affinity proteomics. Biochim Biophys Acta Proteins Proteom. 2017;1865(8):985-996. DOI: 10.1016/j.bbapap.2017.03.007.
37. Winter G, Milstein C. Man-made antibodies. Nature. 1991;349(6307):293-299. DOI: 10.1038/349293a0.
38. Chames P, Baty D. Antibody engineering and its applications in tumor targeting and intracellular immunization. FEMS Microbiol Lett. 2000;189(1):1-8. DOI: 10.1111/j.1574-6968.2000.tb09197.x.
39. Guglielmi L, Martineau P. Expression of single-chain Fv fragments in *E. coli* cytoplasm. Methods Mol Biol. 2009;562:215-224. DOI: 10.1007/978-1-60327-302-2_17.
40. de Marco A. Strategies for successful recombinant expression of disulfide bond-dependent proteins in *Escherichia coli*. Microb Cell Fact. 2009;8:26,1-18. DOI: 10.1186/1475-2859-8-26.
41. Sørensen HP, Mortensen KK. Soluble expression of recombinant proteins in the cytoplasm of *Escherichia coli*. Microb Cell Fact. 2005;4(1):1,1-8. DOI: 10.1186/1475-2859-4-1.
42. Salinas G, Pellizza L, Margenat M, Fló M, Fernández C. Tuned *Escherichia coli* as a host for the expression of disulfide-rich proteins. Biotechnol J. 2011;6(6):686-699. DOI: 10.1002/biot.201000335.
43. Kane JF. Effects of rare codon clusters on high-level expression of heterologous proteins in *Escherichia coli*. Curr Opin Biotechnol. 1995;6(5):494-500.

DOI: 10.1016/0958-1669(95)80082-4.
44. Novagen, Inc. 2004 EMD Biosciences, Inc. Competent Cells. Available at: https://www.scribd.com/document/59544787/Competent-Cells-Novagen-Detailed.
45. Shafiee F, Rabbani M, Jahanian-Najafabadi A. Optimization of the expression of DT386-BR2 fusion protein in *Escherichia coli* using response surface methodology. Adv Biomed Res. 2017;6:22,1-6. DOI: 10.4103/2277-9175.201334.
46. Ahmadzadeh M, Farshdari F, Behdani M, Nematollahi L, Mohit E. Cloning, expression and one-step purification of a novel IP-10-(anti-HER2 scFv) fusion protein in *Escherichia coli*. Int J Pept Res Ther. 2021;27(1):433-446. DOI: 10.1007/s10989-020-10100-z.
47. Akbari V, Mir Mohammad Sadeghi H, Jafrian-Dehkordi A, Abedi D, Chou CP. Functional expression of a single-chain antibody fragment against human epidermal growth factor receptor 2 (HER2) in *Escherichia coli*. J Ind Microbiol Biotechnol. 2014;41(6):947-956. DOI: 10.1007/s10295-014-1437-0.
48. Atroshenko DL, Sergeev EP, Golovina DI, Pometun AA. Additivities for soluble recombinant protein expression in cytoplasm of *Escherichia coli*. Fermentation. 2024;10(3):120,1-12. DOI: 10.3390/fermentation10030120.
49. Malakar P, Venkatesh KV. Effect of substrate and IPTG concentrations on the burden to growth of *Escherichia coli* on glycerol due to the expression of Lac proteins. Appl Microbiol Biotechnol. 2012;93(6):2543-2549. DOI: 10.1007/s00253-011-3642-3.
50. Farshdari F, Ahmadzadeh M, Nematollahi L, Mohit E. The improvement of anti-HER2 scFv soluble expression in *Escherichia coli*. Braz J Pharm Sci. 2020;56:e17861,1-8. DOI: 10.1590/s2175-97902019000317861.
51. Barkhordari F, Sohrabi N, Davami F, Mahboudi F, Garoosi YT. Cloning, expression and characterization of a HER2-alpha luffin fusion protein in *Escherichia coli*. Prep Biochem Biotechnol. 2019;49(8):759-766. DOI: 10.1080/10826068.2019.1608447.
52. Liu M, Wang B, Wang F, Yang Z, Gao D, Zhang C, *et al*. Soluble expression of single-chain variable fragment (scFv) in *Escherichia coli* using superfolder green fluorescent protein as fusion partner. Appl Microbiol Biotechnol. 2019;103(15):6071-6079. DOI: 10.1007/s00253-019-09925-6.
53. Rasooli F, Hashemi A. Efficient expression of EpEX in the cytoplasm of *Escherichia coli* using thioredoxin fusion protein. Res Pharm Sci. 2019;14(6):554-565. DOI: 10.4103/1735-5362.272564.
54. Singh A, Upadhyay V, Upadhyay AK, Singh SM, Panda AK. Protein recovery from inclusion bodies of *Escherichia coli* using mild solubilization process. Microb Cell Fact. 2015;14:41,1-10. DOI: 10.1186/s12934-015-0222-8.
55. de Groot NS, Ventura S. Effect of temperature on protein quality in bacterial inclusion bodies. FEBS Lett. 2006;580(27):6471-6476. DOI: 10.1016/j.febslet.2006.10.071.
56. Koçer İ, Cox EC, DeLisa MP, Çelik E. Effects of variable domain orientation on anti-HER2 single-chain variable fragment antibody expressed in the *Escherichia coli* cytoplasm. Biotechnol Prog. 2021;37(2):e3102,1-19. DOI: 10.1002/btpr.3102.
57. Zhu YQ, Tong WY, Wei DZ, Zhou F, Zhao JB. Environmental stimuli on the soluble expression of anti-human ovarian carcinoma × anti-human CD3 single-chain bispecific antibody in recombinant *Escherichia coli*. Biochem Eng J. 2007;37(2):184-191. DOI: 10.1016/j.bej.2007.04.010.
58. Schütz A, Bernhard F, Berrow N, Buyel JF, Ferreira-da-Silva F, Haustraete J, *et al*. A concise guide to choosing suitable gene expression systems for recombinant protein production. STAR Protoc. 2023;4(4):102572,1-16. DOI: 10.1016/j.xpro.2023.102572.
59. Zarei N, Vaziri B, Shokrgozar MA, Mahdian R, Fazel R, Khalaj V. High efficient expression of a functional humanized single-chain variable fragment (scFv) antibody against CD22 in Pichia pastoris. Appl Microbiol Biotechnol. 2014;98(24):10023-10039. DOI: 10.1007/s00253-014-6071-2.
60. Jellusova J, Nitschke L. Regulation of B cell functions by the sialic acid-binding receptors siglec-G and CD22. Front Immunol. 2012;2:96,1-14. DOI: 10.3389/fimmu.2011.00096.